Available online at www.sciencedirect.com
ScienceDirect
Journal of Power Sources 161 (2006) 1435–1442
JOURNAL OF POWER SOURCES
www.elsevier.com/locate/jpowsour

Electrochemical characterization of $LaNi_{5-x}Al_x$ ($x = 0.1$–0.5) in the absence of additives

Jun Liu, Yifu Yang*, Peng Yu, Yan Li, Huixia Shao

College of Chemistry and Molecular Science, Wuhan University, Wuhan 430072, China

Received 4 March 2006; received in revised form 22 May 2006; accepted 24 May 2006
Available online 3 July 2006

Abstract

The electrochemical performance of $LaNi_{5-x}Al_x$ ($x = 0.1$–0.5) hydrogen storage alloys was quickly and systematically evaluated by powder microelectrode (PME) technique. X-ray diffraction (XRD) and X-ray photo-electron spectroscopy (XPS) studies were also carried out for a better understanding of the effect of Al partial substitution for Ni on the alloy's performance. PME study results show that Al partial substitution for Ni improves both the cycling performance and the anti-electro-oxidation ability of the alloys; however, it prolongs the alloy activation process, decreases the maximum discharge ability and enhances the polarization of the alloy electrode. The alloy decay mainly behaves as the capacity reduction with the time, but the maximum discharge ability almost keeps constant during the service life. The changes of both the physical and the chemical properties of the alloys resulted from Al partial substitution for Ni are the main factors which lead to the changes of the electrochemical performance of the alloys.

Keywords: Hydrogen storage alloy; $LaNi_{5-x}Al_x$; Electrochemical performance; Powder microelectrode (MPE)

1. Introduction

$LaNi_5$ and its B-site substituted derivatives, used as anode materials of "green" Ni–MH batteries, have been studied by many scientific researchers [1–16]. Among the elements for B-site substitution, Al is an effective one to improve the overall performance of the alloy [2–7,13–16]. Most of the previous works concerning the effect of Al partial substitution were carried out on composite electrodes prepared by mixing powdery alloy with electric conducting additive and polymer binder. Although composite electrodes were widely used in battery research and manufacture, the great difference in properties between the alloys and the additives makes it impossible to study the intrinsic electrochemical behavior of the alloy. Additionally, the high double layer capacitance of the composite electrodes prevents the rapid evaluation of the electrochemical performance of the alloy materials; and so the alloy composite electrodes always suffer from the calendar corrosion which could seriously distort the genuine electrochemical performance of the alloy.

In order to circumvent the difficulties stated above, powder microelectrode (PME) technique which avoids the use of additives was developed by Cha et al. [17]. PME has been proved to be an effective way for the straightforward study of the properties of electroactive materials [17–21], including the hydrogen storage alloys [17,20,21]. One outstanding advantage of the technique is that even the cycle life testing time is fantastically short. Thus, the material studied by this technique can escape the influence of calendar corrosion. Recently, Merzouki et al. [20] investigated several hydrogen storage alloys ($LaNi_5$, $LaNi_{4.7}Al_{0.3}$, $LaNi_{4.6}Mn_{0.4}$, $LaNi_{4.25}Co_{0.75}$ and $LaNi_{3.55}Co_{0.75}Mn_{0.4}Al_{0.3}$) by PME (nominated as "CME" in Ref. [20]) technique. However, systematical study of $LaNi_{5-x}Al_x$ series by PME technique has not been reported yet. In this work, the overall electrochemical performance of $LaNi_{5-x}Al_x$ ($x = 0.1$–0.5) was characterized by PME technique. XRD and XPS studies were also carried out for better understanding the effect of Al partial substitution for Ni on the electrochemical performance of the alloy. The reasons causing the difference of the properties between the alloys

* Corresponding author. Tel.: +86 27 8721 8624; fax: +86 27 68754067.
E-mail address: yang-y-f1@vip.sina.com (Y. Yang).

0378-7753/$ – see front matter © 2006 Elsevier B.V. All rights reserved.
doi:10.1016/j.jpowsour.2006.05.037

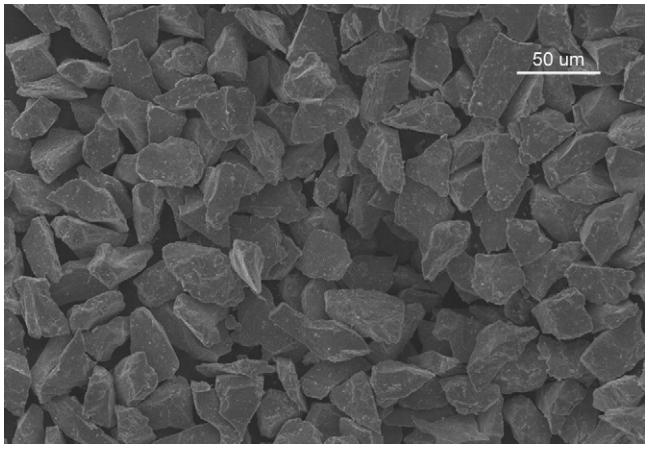

Fig. 1. SEM view of the alloy particles.

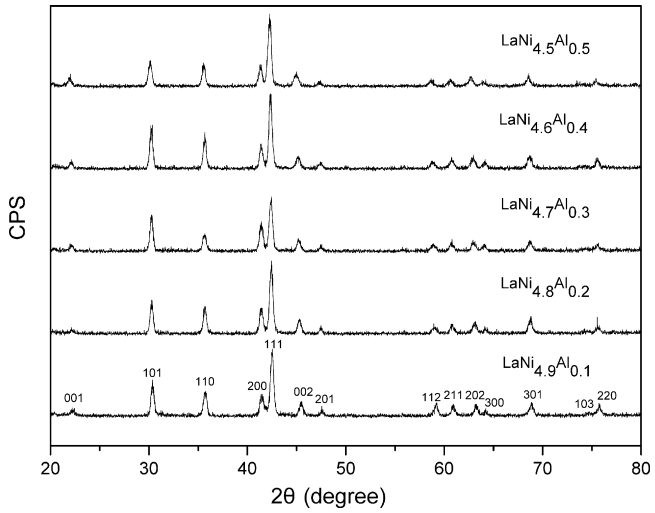

Fig. 2. XRD patterns of $LaNi_{5-x}Al_x$ ($x = 0.1$–0.5).

substituted by different amount of Al were also discussed in the final part of this paper.

2. Experimental

$LaNi_{5-x}Al_x$ ($x = 0.1$–0.5) were prepared by magnetic levitation melting method. The crystal structures of the hydrogen storage alloys were identified by an X-ray diffractometer (XRD-6000, Shimadzu, Japan) with Cu Kα radiation ($\lambda = 1.54056$ Å).

The alloy powder microelectrode was prepared following the procedure described in Ref. [17] except that the graphite powder (electronic connector between the Pt wire and the Cu leader) was replaced by tin; this improvement reduces the whole electronic resistance of the electrode from ca. 10 Ω [18] to ca. 0.5 Ω. The depth of the microcavity (l) was approximately two times of the Pt wire radius ($r = 30$ μm). The SEM view of the alloy particles is shown in Fig. 1, the particles have an irregular shape (which is similar to that reported in Ref. [21]) and their size is in the range of ca. 25–40 μm. After being packed with the alloy particles/powder, the microcavity of the PME was checked with a stereoscope (SM, Tech. Instrument Ltd., Beijing) to ensure that it had been fully filled. The powder in the microcavity can be unloaded by ultrasonication after experiment.

Electrochemical experiments were carried out in a classical three-electrode cell with an electrochemistry work station (CHI660A, Chenhua instrument Ltd., Shanghai). The working electrode was an alloy PME, the counter electrode was a Pt foil and the reference electrode was a home-made Hg/HgO electrode filled with 6 mol L^{-1} KOH solution. All potentials reported in this paper are referred to this reference electrode. The electrolyte was a degassed 6 mol L^{-1} KOH solution.

Before and after the electrochemical cycling of $LaNi_{4.7}Al_{0.3}$ (typical sample of $LaNi_{5-x}Al_x$), the relative concentration and the chemical states of Al on the alloy surface were analyzed by a XPS instrument (XSAM800, KRATOS) with the Mg Kα target at 1253.6 eV and 16 mA.

3. Results

3.1. XRD patterns and cell parameters of $LaNi_{5-x}Al_x$

X-ray diffraction (XRD) was used to characterize the microstructure and to measure the cell parameters of the hydrogen storage alloys. Fig. 2 shows the XRD patterns of $LaNi_{5-x}Al_x$. The patterns depict that all the alloys crystallize in the $CaCu_5$-type hexagonal structure. Table 1 lists the lattice parameters and the cell volume of the alloys. It can be seen that both the lattice parameters (a, c) and the cell volume of $LaNi_{5-x}Al_x$ increase with increasing Al content, which can be ascribed to the larger atomic radius of Al (1.43 Å) than that of Ni (1.24 Å). By further plotting the cell volume against x in $LaNi_{5-x}Al_x$, it is found that the cell volume increases linearly with increasing the amount of Al in the alloy (shown in Fig. 3). The result agrees very well with that reported by Zhang et al. [16].

3.2. Voltammograms recorded with PME

Careful experiment showed that upper potential limit exceeding −0.2 V in cyclic voltammetry will cause irreversible loss of the hydrogen storage capacity of the alloys, so CV was carried

Table 1
Lattice parameters and cell volume of $LaNi_{5-x}Al_x$

	$LaNi_{4.9}Al_{0.1}$	$LaNi_{4.8}Al_{0.2}$	$LaNi_{4.7}Al_{0.3}$	$LaNi_{4.6}Al_{0.4}$	$LaNi_{4.5}Al_{0.5}$
a (Å)	5.0201	5.0227	5.0270	5.0301	5.0336
c (Å)	3.9831	3.9946	4.0041	4.0133	4.0208
Cell volume (Å^3)	86.9326	87.2720	87.6301	87.9398	88.2268

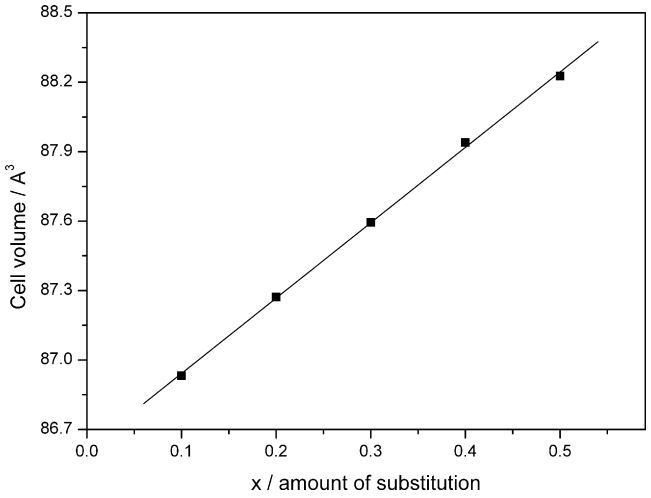

Fig. 3. The variation of cell volume with x in $LaNi_{5-x}Al_x$ ($x = 0.1$–0.5).

out on PME in the potential range of −1.15 to −0.3 V. The scan rate of the potential was set as 50 mV s^{-1}, same as in the previous study [20,21].

Fig. 4 shows the typical voltammogram of $LaNi_5$-type PME, the cathodic current peak C and the anodic current peak A reflect the details of the alloy charge/discharge process, respectively. It is also shown in Fig. 4 that the current response of Pt current collector as the background (dotted line) is negligible when compared with that of the alloy material (solid line). The part of the solid curve with the condition of $I > 0$ in Fig. 4 represents the discharge process of the alloy, so the discharge capacity (Q_d) can be calculated according to Eq. (1):

$$Q_d = \frac{S_a + 2S_b}{v} \quad (1)$$

where $S_a + 2S_b$, schematically shown in the inset of Fig. 4, is the integrating area of $I > 0$ part of the current curve; v is the scan rate of the potential.

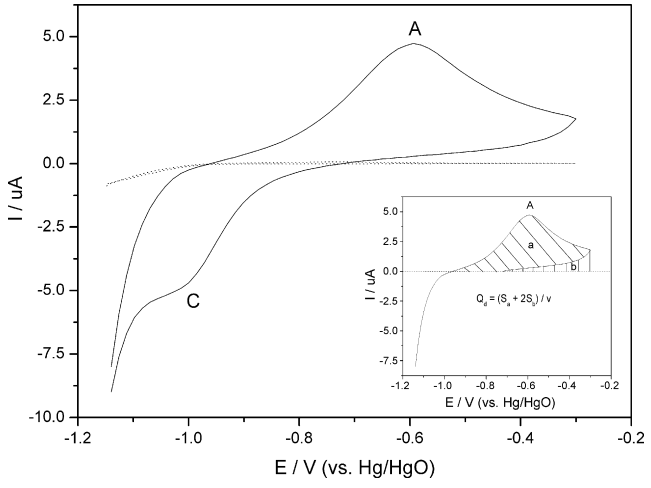

Fig. 4. Typical cyclic voltammogram of $LaNi_5$-type hydrogen storage alloy PME. Potential range: −1.15 to −0.3 V; scan rate: 50 mV s^{-1}; solid line: the voltammogram of the alloy powder; dotted line: the voltammogram of the Pt current collector; dashed line: the base line in the inset is for the integration of the anodic current peak.

Multi-cycle voltammograms of $LaNi_{5-x}Al_x$ ($x = 0.1$–0.5) are shown in Fig. 5. Plenty of information (such as peak current, peak potential, etc.) can be obtained from this figure.

3.3. Activation cycle

The appearance of the maximum discharge capacity ($Q_{d\text{-max}}$) denotes the accomplishment of the activation of the hydrogen storage alloy. The number of cycles needed for Q_d to reach $Q_{d\text{-max}}$ characterizes the activation cycle of the alloy. Fig. 6 shows that the activation cycle of $LaNi_{5-x}Al_x$ increases with increasing x from 0.1 to 0.5. The result indicates that Al partial substitution for Ni prolongs the activation process of the alloy.

3.4. Cycling performance

After activation, long cycle life test was carried out on $LaNi_{5-x}Al_x$ alloy electrode. Since it is difficult to determine the exact amount of material packed into the microcavity, normalized charge (defined as $Q_{norm} = Q_d/Q_{d\text{-max}}$) was used to describe the relative discharge capacity and Q_{norm} versus cycle number curves was used to illustrate the decay process of the alloy material [20,21]. Fig. 7 shows Q_{norm} versus cycle number curves of $LaNi_{5-x}Al_x$. It is obvious that the decay rate of Q_{norm} of $LaNi_{5-x}Al_x$ decreases with increasing the x value. The result implies that Al partial substitution for Ni helps to improve the cycling performance of the alloy.

3.5. Maximum discharge ability

Maximum discharge ability is an important index for the evaluation of hydrogen storage alloy performance. In cyclic voltammograms, the anodic peak current (I_p) represents the maximum change of the electric charge in unit time in the discharge process, thus the maximum discharge ability can be featured by I_p/Q_d (%), which represents the maximum percentage of the discharged capacity in unit time (% s^{-1}). After the alloys were fully activated, the data of I_p/Q_d of $LaNi_{5-x}Al_x$ was plotted against cycle number as shown in Fig. 8. The figure depicts that I_p/Q_d of the alloys holds constant when increasing the cycle number, but it decreases with increasing the amount of Al substitution. The results manifest that: (1) the maximum discharge ability of all the alloys does not degrade during the capacity decay process; (2) Al partial substitution for Ni decreases the maximum discharge ability of the alloy.

3.6. Anodic peak potential (E_p)

The anodic peak potential (E_p) characterizes the polarization behavior of the alloy electrode during the discharge process. The polarization of an electrode includes three components, i.e., the ohmic polarization (η_{ohm}), the electrochemical polarization (also named as charge transfer polarization, η_{ct}) and the concentration polarization (η_{conc}). According to Ref. [22], η_{ohm} increases with increasing the product of I_p and R_{ohm} (the sum of the electric resistance of the electrode and the solution); η_{ct} is proportional to $\ln I_p$, and η_{conc} varies with the variation of

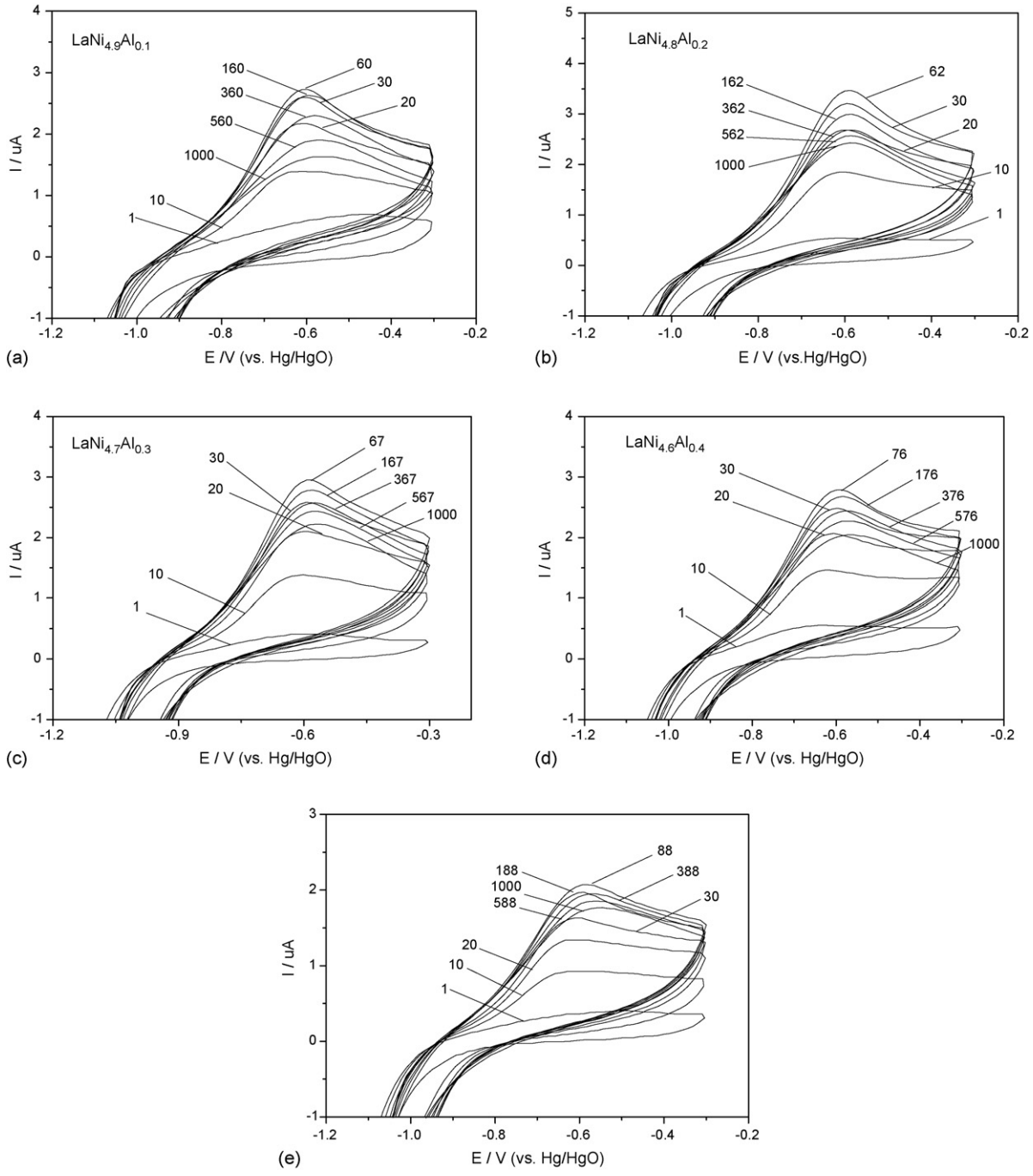

Fig. 5. Cyclic voltammograms of $LaNi_{5-x}Al_x$ ($x = 0.1$–0.5). Potential range: -1.15 to -0.3 V; scan rate: 50 mV s^{-1}.

$\ln(i_L/(i_L - i_p))$, where $i_p = 2.69 \times 10^5 n^{3/2} v^{1/2} D_H^{1/2} C_H^0$ is the anodic peak current density [23] (n is the number of the electrons transferred during the electrochemical reaction, v is the scan rate of the potential, D_H is the diffusion coefficient of H atom and C_H^0 is the concentration of H in the alloy bulk); $i_L = 4nFD_H C_H^0/(\pi r + 4l)$ is the limiting diffusion current density based on PME model [22]. Therefore, $\ln[i_L/(i_L - i_p)] = \ln[1/1 - 0.7(\pi r + 4l)v^{1/2} D_H^{-1/2}]$ is a constant. This indicates that η_{conc} keeps unchanged during the electrochemical cycling of the alloy. Thus, E_p is only governed by η_{ct} and η_{ohm}. Fig. 9 illustrates the relation of E_p of $LaNi_{5-x}Al_x$ alloy electrodes and the cycle number. One can see that during the first tens of cycles (corresponding to activation stage), E_p of all $LaNi_{5-x}Al_x$ alloy electrodes shifts positively with increasing the cycle number. This should be ascribed to the increase of I_p which results in the increase of both η_{ct} and η_{ohm} at the activation stage. While after the initial tens of cycles (corresponding to the decay stage of I_p), E_p of the alloy electrodes shifts positively with increasing the cycle number and with increasing the x value. The above results imply that: (1) Al partial substitution for Ni enhances the polarization of the alloy electrode during the anodic process; (2) some other reaction mechanism may be

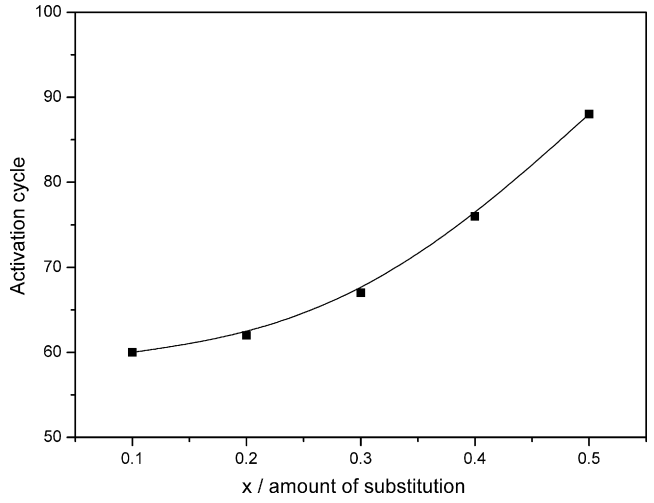

Fig. 6. Activation cycles vs. x in $LaNi_{5-x}Al_x$ ($x = 0.1$–0.5).

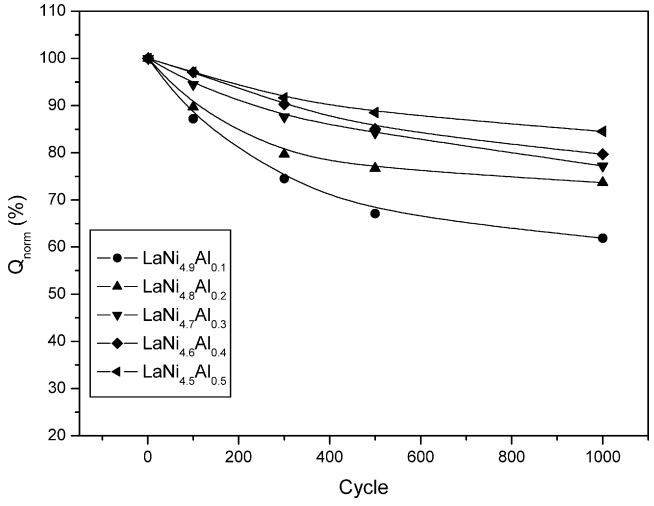

Fig. 7. The capacity decay curves of $LaNi_{5-x}Al_x$ ($x = 0.1$–0.5). Potential range: −1.15 to −0.3 V; scan rate $v = 50\,mV\,s^{-1}$.

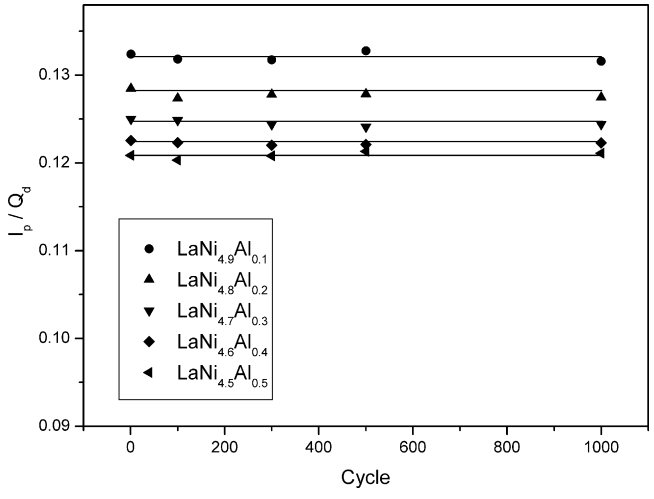

Fig. 8. Maximum discharge ability I_p/Q_d vs. cycle number curves of $LaNi_{5-x}Al_x$ ($x = 0.1$–0.5).

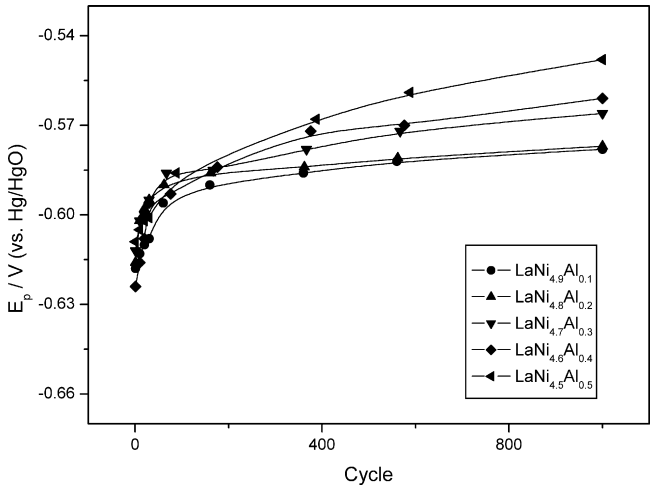

Fig. 9. The anodic peak potential, E_p vs. cycle number curves of $LaNi_{5-x}Al_x$ ($x = 0.1$–0.5).

involved in $LaNi_{5-x}Al_x$ decay process, and this will be discussed later.

3.7. Anti-electro-oxidation ability

When Ni–MH battery used in over-discharge or high rate discharge condition, the potential of the alloy anode would shift positively. If this potential shift is too remarkable, the alloy material would be electro-oxidized and the alloy capacity would decay irreversibly. So studying the effect of the element substitution in B-site on the anti-electro-oxidation ability of AB_5 alloy is quite meaningful. However, previous works paid little attention to this aspect.

The condition for simulating the electro-oxidation of the alloys can be created by elevating the upper potential limit of the cyclic voltammetry to a proper value. When the upper potential limit is set as 0 V, the hydrogen storage capacity of $LaNi_{4.9}Al_{0.1}$ (reflected by the discharge capacity Q_d which was calculated with the same method described in Section 3.2) decreases rapidly with increasing the cycle number (see Fig. 10), which indicates

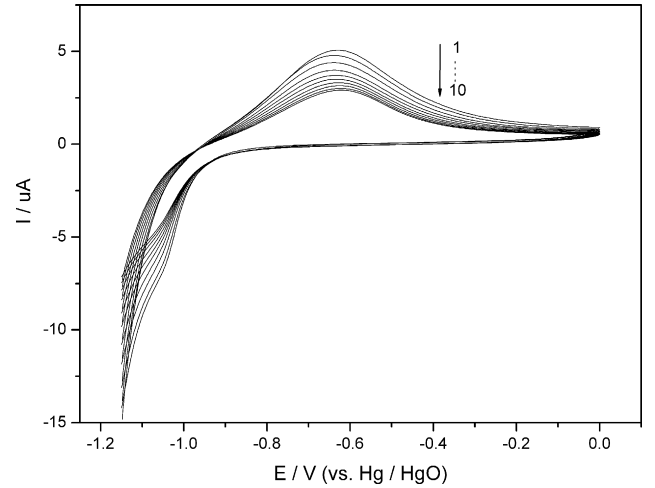

Fig. 10. Cyclic voltammogram of $LaNi_{4.9}Al_{0.1}$. Potential range: −1.15–0 V; scan rate: $50\,mV\,s^{-1}$.

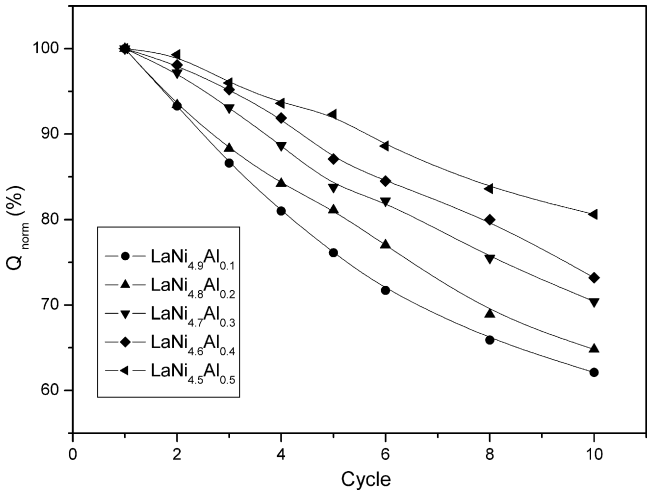

Fig. 11. The decay curves of $LaNi_{5-x}Al_x$ ($x = 0.1$–0.5). Potential range: −1.15–0 V; scan rate $v = 50\,mV\,s^{-1}$.

that the alloy has been seriously oxidized. Similar phenomena were also observed on other $LaNi_{5-x}Al_x$ PME. Q_d versus cycle number curves of $LaNi_{5-x}Al_x$ are shown in Fig. 11. It depicts that Al partial substitution for Ni slows down the decay rate of Q_d. This fact suggests that the anti-electro-oxidation ability of the alloys can be improved by partial substitution of Ni with Al.

3.8. Chemical states of Al on $LaNi_{4.7}Al_{0.3}$ surface

Chemical states of the alloy surface elements are crucial not only to the electric conductivity but also to the explanation of the corrosion mechanism [25]. Chemical states of surface La and Ni are unanimously reported as $La(OH)_3$, Ni and $Ni(OH)_2$, respectively [10,25], while those of surface Al are still in debate. Sakai et al. [6,7] deemed that a protective Al oxide layer was formed on $LaNi_{4.5}Al_{0.5}$ surface during electrochemical cycling and this layer prevented the alloy from fast decay. Whereas Maurei et al. [10] reported that neither Al nor Al oxide was observed with EDX on the electrochemically cycled $MmNi_{3.55}Co_{0.75}Mn_{0.4}Al_{0.3}$ surface. However, the chemical resolution of EDX is not high enough for light element (such as Al) analysis. Comparably, XPS is more sensitive to the detection of surface Al. By using XPS, Meli et al. [25] found the existence of Al on $LaNi_{4.7}Al_{0.3}$ surface after 30 cycles of galvanostatic charge-discharge, but they proposed that no passive Al oxide existed on the alloy surface. Nevertheless, by careful examining the XPS data in their paper, it can be found that the XPS curves of electrochemically cycled alloy involved the information of both the metallic Al and Al oxide. In order to identify the chemical states of surface Al, XPS study was carried out on the surface of $LaNi_{4.7}Al_{0.3}$ alloy with different treatments. Fig. 12 shows the XPS curves measured on the surface of $LaNi_{4.7}Al_{0.3}$ electrode before CV, after CV for 10 h and for a week, respectively. In the measured binding energy scope, the solid line (the original curve recorded by XPS) involves all the information of surface Al and Ni. The dotted lines are the characteristic curves of the surface elements with different chemical states. The dashed line, obtained by adding up the dotted lines, is the fitted curve for

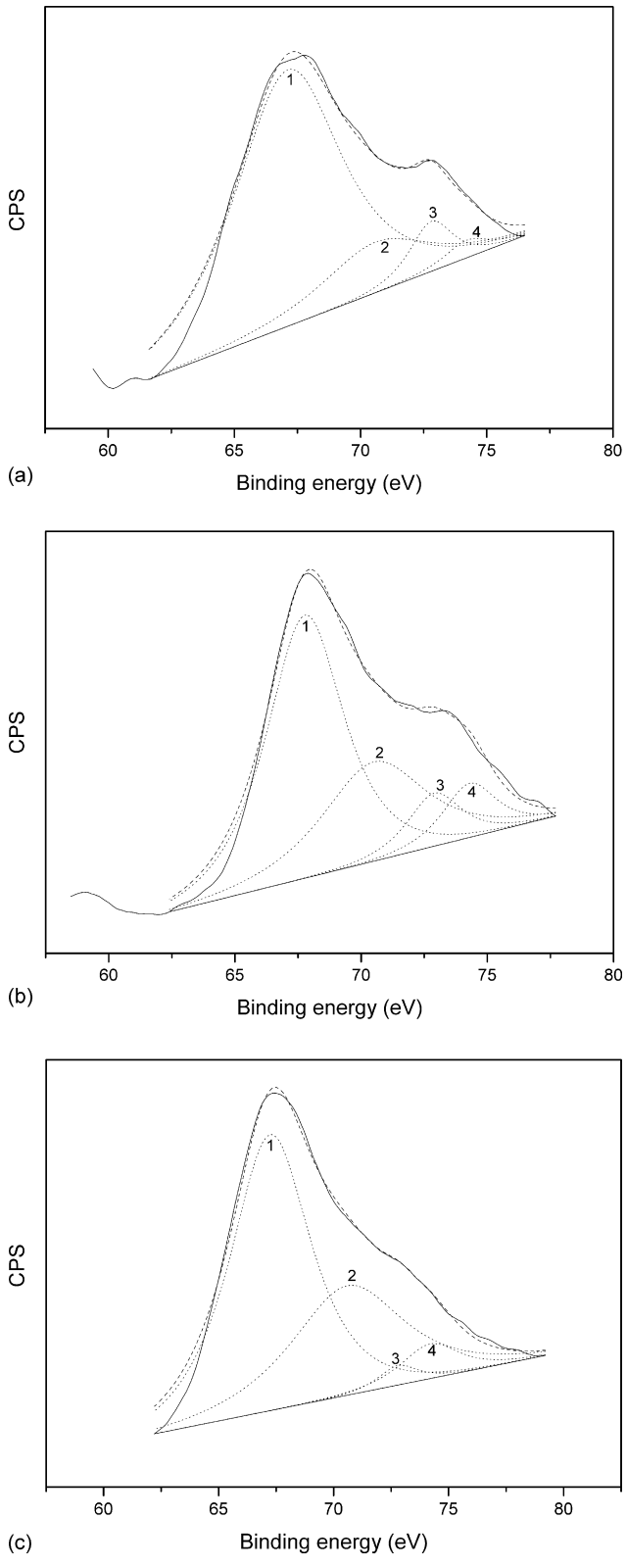

Fig. 12. XPS of $LaNi_{4.7}Al_{0.3}$: (a) fresh sample; (b) CV for 10 h; (c) CV for a week. (—) The original curve recorded with XPS, includes all information of surface Al and Ni; (. . .) the characteristic curve of different chemical states of Al or Ni; (- - -) the fitted curve, added up by the dotted curves, for the simulation of the original one.

Table 2
Relative ratio of surface products of $LaNi_{4.7}Al_{0.3}$ alloy with different treatments

$LaNi_{4.7}Al_{0.3}$	$(Al + Al_2O_3):(Ni + Ni(OH)_2)$	$Al:Al_2O_3$	$Ni:Ni(OH)_2$
Fresh sample	0.085	2.83	5.07
CV for 10 h	0.187	0.98	2.00
CV for a week	0.082	0.38	1.82

simulating the solid line. The fact that the dashed line almost overlaps the solid line indicates that the original curve can be disassembled as several different characteristic curves. From these characteristic curves, we can obtain both the chemical and compositional information of surface Al and Ni. According to the potential-pOH diagram [26,27], Al_2O_3 and $Ni(OH)_2$ are more stable than $Al(OH)_3$ and NiO in alkaline solution individually, so dotted lines with peak potential at ca. 72.8, 74.2, 67.5 and 70.6 eV are corresponding to the characteristic curves of Al (dotted line 3), Al_2O_3 (dotted line 4), Ni (dotted line 1) and $Ni(OH)_2$ (dotted line 2), respectively [28]. Table 2 lists the relative ratio of surface products of $LaNi_{4.7}Al_{0.3}$ with different treatments. The relative ratio of the surface products of Al to Ni on the fresh $LaNi_{4.7}Al_{0.3}$ surface increases from 0.085 to 0.187 after 10 h cyclic voltammety and then decrease to 0.082 after further cycling the electrode for a week. The result indicates that the relative concentration of surface Al products experiences a firstly increasing and then decreasing process during the electrochemical cycling of the alloy electrode. The initial enrichment of surface Al products should be ascribed to the formation of Al_2O_3 and the following decrease of Al concentration should be attributed to the calendar corrosion/dissolution of Al product [10,20]. Table 2 also shows that the relative ratio of the metallic state to the oxidative state of the surface element (both Al and Ni) decreases with increasing the time of the electrochemical cycling, but the decrease rate of Ni (from 5.07 to 1.82 for a week electrochemical cycling) is slower than that of Al (from 2.83 to 0.38 for a week electrochemical cycling). The results indicate that: (1) the oxidation of both Al and Ni occurs on the alloy surface during electrochemical cycling; (2) the oxidation rate of surface Ni is much slower than that of surface Al.

4. Discussions

4.1. Physical properties

Al partial substitution for Ni leads to the change of the physical properties of the alloy which play an important role in deciding the electrochemical performance of the alloy. Firstly, the substitution lowers the Vickers hardness of the alloy [6]. Sakai et al. [6] reported that higher Vickers hardness can cause higher pulverization rate of the alloy. It is known that pulverization can increase the real surface area of the alloy. Thus, the lowered Vickers hardness of the alloy resulted from Al partial substitution for Ni contributes to both the slower activation rate and the better cycling performance. Secondly, the substitution increases the cell volume of the alloy. On the one hand, the increase of the cell volume decreases the lattice expansion ratio of unit cell and further decreases the pulverization rate of the alloy [9]. So it also contributes to both the slower activation rate and the better cycling performance. On the other hand, the increase of the cell volume leads to both the decrease of the hydrogen plateau pressure [2,3] and the increase of the stability of the alloy hydride, and so results in the decrease of the hydrogen diffusion coefficient [29]. Since the diffusion of H is the rate determining step (RDS) of the discharge process of the B-site mono-substituted $LaNi_5$-type alloy [24], the increase of the cell volume decreases the maximum discharge ability of the alloy. Thirdly, the substitution changes the affinity of the lattice to H atoms, which is reflected by the interaction between the metals in the unit cell and H atoms. The interaction between a metal and H atoms can be judged by the magnitude of the formation heat of the metal hydride and the stronger interaction results in the smaller the diffusion coefficient of hydrogen in the alloy bulk [30]. Since the formation heat of $AlH_{0.5}$ ($-7\ kJ\ mol^{-1}$) is larger than that of $NiH_{0.5}$ ($-3\ kJ\ mol^{-1}$) [31], the interaction between Al and H atoms is stronger than that between Ni and H. Thus, the affinity of the lattice to H atoms increases when increasing Al concentration in the unit cell. As the result, the diffusion coefficient of hydrogen and the maximum discharge ability of the alloy decrease.

4.2. Chemical properties

Al partial substitution for Ni also results in the variation of the chemical properties of the alloy. The chemical properties affect the electrochemical performance of the alloy always through the surface effect. XPS results show that Al_2O_3 forms on the alloy surface during electrochemical cycling. The formation of the surface Al_2O_3 increases the contact resistance between the alloy particles and so enhances the polarization of the alloy electrode. In addition, the amount of Al_2O_3 increases with increasing the cycle number, and thus it increases the polarization of the alloy electrode during the decay process. However, the better cycling performance of the alloy with Al partial substitution for Ni can't be ascribed to the formation of a passive Al_2O_3 film, because the ratio of Al on alloy surface is too small. Since the electronegativity value of Al ($\chi = 1.61$) is smaller than that of Ni ($\chi = 1.91$), it can be considered that Al (anode) and Ni (cathode) forms many microprimary cells on the alloy surface in the alkaline solution. During the alloy corrosion process, Al anode is oxidized into Al_2O_3 and Al_2O_3 slowly dissolves into the solution, while oxidative species (such as O_2) is reduced on Ni cathode. In this process, electrons flowing from Al anode to Ni cathode protect Ni from oxidation. Since a considerable amount of metallic Al still exists on the alloy surface after 10 h electrochemical cycling (see Table 2), the primary cell effect may contribute to the long cyclic life of $LaNi_{5-x}Al_x$ alloy in this work. It should be mentioned that both Al and Al_2O_3 suffers the calendar dissolution in the alkaline solution, so this type of contribution to the cycling performance is minor when the alloy is tested in galvanostatic charge–discharge mode (the test time in this mode is very long). The primary cell effect can also explain the improvement of the anti-electrooxidation ability of the alloy made by Al partial substitution for Ni.

5. Conclusions

The electrochemical performance of $LaNi_{5-x}Al_x$ (x = 0.1–0.5) was rapidly evaluated by means of PME. XRD and XPS studies were also carried out for a better understanding of the effect of Al partial substitution for Ni on the alloy's performance. According to the results, following conclusions can be drawn:

1. Al partial substitution for Ni improves both the cycling performance and the anti-electro-oxidation ability; but prolongs the alloy activation process, decreases the maximum discharge ability and enhances the polarization of the alloy electrode.
2. The alloy decay mainly behaves as the capacity reduction with the time, but the maximum discharge ability almost keeps constant during the service life.
3. Both metallic and oxidative states of Al were detected on $LaNi_{4.7}Al_{0.3}$ surface; the formation of surface Al_2O_3 should be responsible for the enhanced polarization of $LaNi_{5-x}Al_x$ alloy electrode.
4. Al partial substitution for Ni leads to the changes of both the physical and the chemical properties of the alloy. These changes are the intrinsic reason resulting in the changes of the electrochemical performances of the alloy: The decrease of Vickers hardness, the increase of the cell volume and the primary cell effect contribute to the better cycling performance of the alloy. The prolonged activation process of the alloy should be attributed to the lowered Vickers hardness and the increased cell volume. The decrease of the maximum discharge ability of the alloy should be ascribed to the increase of both the cell volume and the affinity of the lattice of H atoms. The improvement of the alloy's anti-electro-oxidation ability should also be attributed to the primary cell effect.

Acknowledgement

The financial support by Chinese National Programs for high technology research and development (Grant No. 2005AA501440) is gratefully acknowledged.

References

[1] J.H.N. Van Vucht, F.A. Kuijpers, H.C.A.M. Bruning, Philips Res. Rep. 25 (1970) 133.
[2] M.H. Mendelsohn, D.M. Gruen, A.E. Dwight, Nature (London) 269 (1977) 45.
[3] M.H. Mendelsohn, D.M. Gruen, A.E. Dwight, J. Less-Common Met. 63 (1979) 193.
[4] J.G. Willems, Philips J. Res. 39 (1984) 1.
[5] J.E. Bonnet, P. Dantzer, H. Dexpert, J.M. Esteva, R. Karnatak, J. Less-Common Met. 130 (1987) 491.
[6] T. Sakai, K. Oguro, H. Miyamura, N. Kuriyama, A. Kato, H. Ishikawa, J. Less-Common Met. 161 (1990) 193.
[7] T. Sakai, H. Miyamura, N. Kuriyama, A. Kato, K. Oguro, H. Ishikawa, J. Less-Common Met. 159 (1990) 127.
[8] D. Chartouni, F. Meli, A. Züttel, K. Gross, L. Schlapbach, Alloys Compd. 241 (1996) 160.
[9] J.J. Reilly, G.D. Adzic, J.R. Johnson, T. Vogt, S. Mukerjee, J. McBreen, J. Alloys Compd. 293 (1999) 569.
[10] F. Maurei, B. Knosp, M. Backhaus-Ricoult, J. Electrochem. Soc. 147 (2000) 78.
[11] J. Han, PhD Dissertation, University of Windsor, 2000.
[12] F. Feng, J. Han, M. Geng, D.O. Northwood, J. Electroanal. Chem. 487 (2000) 111.
[13] R. Baddour-Hadjean, H. Mathlouthi, J.P. Pereira-Ramos, J. Lamloumi, M. Latroche, A. Percheron-Guégan, J. Alloys Compd. 356 (2003) 750.
[14] K. Asano, Y. Hashimoto, T. Iida, M. Kondo, Y. Iijima, J. Alloys Compd. 395 (2005) 201.
[15] R.J. Zhang, Y.M. Wang, M.Q. Lu, D.S. Xu, K. Yang, Acta Materialia 53 (2005) 3445.
[16] R.J. Zhang, M.Q. Lue, D.M. Chen, K. Yang, Jinshu Xuebao 41 (2005) 427.
[17] C.S. Cha, C.M. Li, H.X. Yang, P.F. Liu, J. Electroanal. Chem. 368 (1994) 47.
[18] C.S. Cha, J. Chen, P.F. Liu, Biosens. Bioelectron. 13 (1998) 87.
[19] C. Cachet-Vivier, V. Vivier, C.S. Cha, J.-Y. Nedelec, L.T. Yu, Electrochim. Acta 47 (2001) 181.
[20] A. Merzouki, V. Vivier, C. Cachet-Vivier, J.-Y. Nédélec, L.T. Yu, J.-M. Joubert, A. Percheron-Guégan, J. Power Sources 109 (2002) 281.
[21] V. Vivier, C. Cachet-Vivier, J.-Y. Nédélec, L.T. Yu, J.-M. Joubert, A. Percheron-Guégan, J. Power Sources 124 (2003) 564.
[22] C. Cha, Introduction to the Kinetics of Electrode Processes, 3rd ed., Science Press, Beijing, 2002.
[23] A.J. Bard, L.R. Fualkner, Electrochemical Methods: Fundamentals and Applications, 2nd ed., John Weily & Sons, New York, 2001.
[24] T. Haraki, N. Inomata, H. Uchida, J. Alloys Compd. 293–295 (1999) 407.
[25] F. Meli, L. Schlapbach, J. Less-Common Met. 172–174 (1991) 1525.
[26] H. Senoh, M. Ueda, H. Inoue, N. Furukawa, C. Iwakura, J. Alloys Compd. 266 (1998) 111.
[27] H. Senoh, M. Ueda, N. Furukawa, H. Inoue, C. Iwakura, J. Alloys Compd. 280 (1998) 114.
[28] J.F. Moulder, W.F. Stickle, P.E. Sobol, K.D. Bomben, Handbook of X-ray Photoelectron Spectroscopy, Perkin-Elmer Corporation, USA, 1992.
[29] C. Iwakura, K. Fukuda, H. Senoh, H. Inoue, M. Matsuoka, Y. Yamamoto, Electrochim. Acta 43 (1998) 2041.
[30] M. Morinaga, H. Yukawa, Mater. Sci. Eng. A 329–331 (2002) 268.
[31] J. Kleperis, G. Wójcik, A. Czerwinski, J. Skowronski, M. Kopczyk, M. Beltowska-Brzezinska, J. Solid State Electrochem. 5 (2001) 229.